

Review on Grain Size- and Grain Boundary Phenomenon in Unusual Mechanical Behavior of Ultrafine-Grained Al Alloys

Nguyen Q. Chinh^{1,*1}, Dániel Olasz^{1,2,*2}, Anwar Q. Ahmed^{1,3,*2}, Elena V. Bobruk⁴ and Ruslan Z. Valiev^{4,5}

¹Department of Materials Physics, Eötvös Loránd University, Pázmány Péter sétány 1/A, Budapest, H-1117, Hungary

²Institute for Technical Physics and Materials Science, Centre for Energy Research, Budapest Konkoly-Thege út 29-33, Budapest, 1121, Hungary

³College of Science, University of Kufa, Najaf, 54001, Iraq

⁴Institute of Physics of Advanced Materials, Ufa University of Science and Technology, 32 Zaki Validi str., Ufa, 450076, Russia

⁵Laboratory for Dynamics and Extreme Performance of Advanced Nanostructured Materials, Saint Petersburg State University, 7-9 Universitetskaya nab., St. Petersburg, 199034, Russia

In the last three decades, several severe plastic deformation (SPD) procedures have been developed and applied in materials science to create bulk, ultrafine-grained (UFG) structures. As a consequence of the SPD, not only submicron and even nanometer grain sizes can be obtained, but also new grain boundaries with non-equilibrium structures in a material may be formed. Therefore, both the strength and ductility of the UFG materials can change significantly compared to the coarse-grained counterparts. This review is focused on unusual mechanical behaviors of UFG Al and Al alloys, associated with grain boundary structure and segregations which are responsible for the modification of the Hall-Petch relationship and the so-called size-effect for UFG structure. Unusually high strain rate sensitivity, intensive grain boundary sliding and superplasticity at low temperature are described and surveyed. In addition, innovation potential of these phenomena is also briefly considered. [doi:10.2320/matertrans.MT-MF2022020]

(Received January 31, 2023; Accepted April 17, 2023; Published June 9, 2023)

Keywords: submicron grains, Al alloys, Hall-Petch, grain boundary sliding, strain rate sensitivity, low temperature superplasticity

1. Introduction

In our rapidly developing world, several sectors such as the construction industry, the automotive (airplane, car) industry, or even the manufacturing-, medical equipment- and electronics industries are making new demands on the materials to be used. On the one hand, researchers and manufacturers aim to increase the strength and formability parameters of the existing – traditional – materials. On the other hand, in accordance with economic and environmental protection requirements, the range of applicable raw materials is also expected to be widened. Thanks to technical progress, great opportunities are opening up both in material development and in test methods, for example in the preparation of nano- and submicron crystalline materials,^{1–10} or in monitoring the plastic deformation of samples of different sizes on the micro-scale.^{11–13} In the last three decades, enormous research work has been carried out in materials science in order to produce materials with new compositions and/or new structures for different purposes, as well as in order to learn more and in more detail about the processes related to the strengthening and plastic mechanisms of metal alloys.

The plastic deformation of metals and the micro-mechanisms of strengthening processes are problems that have been studied for several decades and are still not fully clarified. More than 70 years ago, Voce¹⁴ and later Cottrell¹⁵ pointed out that work hardening can strongly increase the strength of pure copper to a saturated – maximum – value, which can be predicted on the basis of experimental stress-strain data. Applying severe plastic deformation (SPD)

procedures that have become known and accepted nowadays, such as Equal Channel Angular Pressing (ECAP),^{1–4} High-Pressure Torsion (HPT),^{1,4,5} Accumulative Roll Bonding (ARB)^{6–8} and others,^{9,10} the microstructure of the metal alloys can be changed significantly into ultrafine-grained (UFG), as the average grain size can be reduced from several microns to very fine submicron. Together with the decrease of the average grain size, the volume fraction of the grain boundaries greatly increases and thus their influence on the material properties and deformation mechanisms may become dominant. The strength of UFG copper exceeds the mentioned predicted maximum by at least 25%. Furthermore, the Hall-Petch equation,^{16,17} which has also been well known for 70 years, also needed to be modified in order to be able to apply it to submicron-structured materials as well.

An important factor in the plasticity of polycrystalline metals is the grain size, which can strongly affect the mechanism of deformation. The mechanism maps for fcc-structured Ni and Al summarized 40 years ago in the much-cited, almost handbook “Maps of Deformation Mechanisms” written by Frost and Ashby¹⁸ were edited for the smallest grain sizes of 1 and 10 μm , respectively. The much lower grain size of 200 nm and 1 μm obtained by using the mentioned SPD techniques have resulted in new phenomena, such as strong twinning¹⁹ or intense grain boundary sliding at room temperature¹¹ in UFG Ni and Al, respectively. These results provide, certainly, new information about the plastic deformation of ultrafine-grained materials.

The aim of this paper is to review the effect of grain size and grain boundary structure on some unusual mechanical behavior of UFG Al and Al alloys. Possible practical significance of intensive grain boundary sliding and the combination of high strength and low temperature superplasticity are also reviewed.

*1Corresponding author, E-mail: chnh@metal.elte.hu

*2Graduate Student, Eötvös Loránd University

2. Effect of Grain Size on Mechanical and Plastic Behaviors of UFG Al and Al Alloys

2.1 Modification of Hall-Petch relationship

The most important motivation for the application of the severe plastic deformation (SPD) procedures comes from the Hall-Petch connection^{16,17)} describing the basic strengthening mechanism in polycrystalline materials. Seventy years ago, basing their conclusions on experimental data obtained on samples of iron, copper and brass,^{16,17,20)} Eric Hall and Norman Petch developed phenomenologically the relationship between yield stress, σ_y , and grain size, d , as:

$$\sigma_y = \sigma_0 + K \cdot d^{-1/2}, \quad (1)$$

where σ_0 is the friction stress (or yield stress of a single crystal) and K is a positive material constant. According to eq. (1) the yield stress and then the strength increase with decreasing grain size. This is the reason why several efforts have been made to obtain sub-micrometer average grain size in conventional materials,^{1–10,21–33)} significantly increasing the strength of these ultrafine-grained materials. It should be noted that the mentioned efforts are always realized by applying different SPD procedures, which can change not only the grain size, but also the characteristics of the microstructures, such as changing the dislocation (in singular) densities, resulting in the segregation and clusters of solute atoms, as well as modifying the distribution of precipitates, etc. All of these characteristics may influence the strengthening mechanisms in the SPD-processed materials.²²⁾

In its original form, with the reciprocal of the root of the grain size ($d^{-1/2}$), the Hall-Petch equation is well established for materials having average grain size higher than 1 μm . Experimental results have shown that eq. (1) no longer holds in the range of lower grain sizes because of some typical problems. Firstly, the value of parameter K in eq. (1) paradoxically changes in the case of submicron grain sizes.^{34–38)} Secondly, eq. (1) is no longer valid at all at grain sizes below approximately 20 nm, where the yield stress decreases with decreasing grain size, causing rather material-softening.^{26,34–38)} The results of 2D molecular dynamics simulations³⁹⁾ have shown that with further decrease of the grain diameter, when $d < 3.5$ nm, this softening behavior, the so-called inverse Hall-Petch effect is replaced by a power-law hardening, which arises from grain mediated shear transformation zones.

Recently,⁴⁰⁾ an appropriate modification of the original Hall-Petch equation has been suggested in order to maintain its applicability for submicron-structured Al and other face-centered cubic (fcc) metals and solid solution alloys, which have almost the same Poisson number ($\nu \approx 1/3$). In this description, the yield stress, σ_y and grain size, d of a given material have been normalized by the corresponding shear modulus, μ and the magnitude, b of the Burgers vector, respectively. Then, the normalized yield stress, σ_y/μ has been related to the normalized grain size, d/b . Considering a dislocation-based model, it has been shown that the normalized yield stress is linearly changing with a power of the normalized grain size, i.e. the conventional Hall-Petch relationship is modified to the form

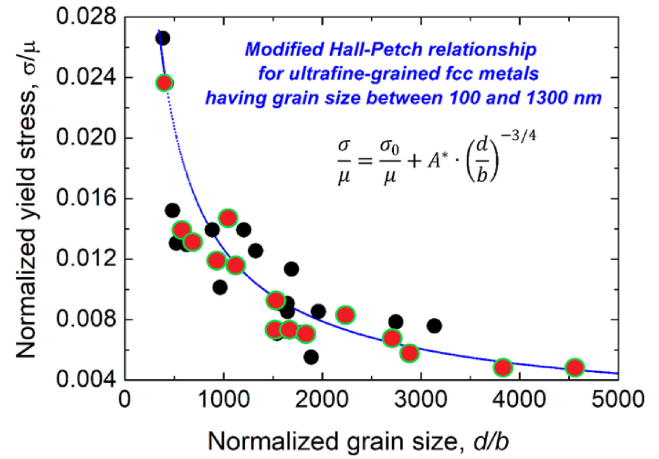


Fig. 1 Presentation of the normalized yield stress-normalized grain size relationship, suggesting a modification of the Hall-Petch relationship for ultrafine-grained fcc metals and solid solutions. Reproduced with permission.⁴⁰⁾ Copyright 2022, Elsevier. The data for Al and Al alloys are red with green border.

$$\frac{\sigma}{\mu} = \frac{\sigma_0}{\mu} + K^* \cdot \left(\frac{d}{b}\right)^{\beta}, \quad (2)$$

where K^* and β are constants depending on the grain size range. Furthermore, in the case of relatively high grain size of $d > 1000$ nm, because of the effect of dislocation pile-ups formed at grain boundaries, the value of β exponent is $-1/2$, giving back the conventional Hall-Petch relationship. For very small grain sizes ($d < 100$ nm), however, no pile-ups can be expected,^{34,36)} resulting in a -1 value for the β exponent.⁴⁰⁾

In the middle range for sub-micron grain size, the value of the exponent β was determined by using experimental data.

Figure 1 shows the relationship between normalized yield stress and normalized grain size for several fcc metals and solid solutions. The best fitting based on eq. (2) has shown that the strength of submicron Al and other fcc metals and solid solutions can be uniformly given by the modification of the original Hall-Petch relationship into the form:

$$\frac{\sigma}{\mu} = \frac{\sigma_0}{\mu} + K^* \cdot \left(\frac{d}{b}\right)^{-3/4}, \quad (3)$$

where $\frac{\sigma_0}{\mu} = 0.0008 \pm 0.0002$ and $K = 2.22 \pm 0.15$. It can be seen that based on the modified eq. (3), the strength of any sub-micron structured fcc metal or solid solution may be estimated if the grain-size is known.

2.2 Intensive grain boundary sliding at room temperature in UFG Al

Together with the strengthening effect, the average grain size has also important role in plastic deformation process, such as superplastic flow, where the main deformation mechanism is grain boundary sliding (GBS).^{41–44)} Under optimal conditions, the steady state flow can be described by the constitutive equation:^{41–43)}

$$\dot{\epsilon} = A^* \frac{D \cdot \mu \cdot b}{k \cdot T} \left(\frac{b}{d}\right)^p \left(\frac{\sigma}{\mu}\right)^{1/m}, \quad (4)$$

where $\dot{\epsilon}$ is the strain rate of the flow, D is the coefficient of grain-boundary diffusion, k is the Boltzmann constant, T is the absolute testing temperature, p is the grain-size exponent, σ is the flow stress of the deformation process, m is the strain rate sensitivity (SRS) and A^* is a dimensionless constant. It can be expected that a decrease of grain size, d should improve the occurrence of steady state flow, even the occurrence of superplastic process at relatively low temperatures and/or relatively high strain rates.

Indeed, experimental results^{36,45–48)} obtained on UFG pure Al deformed plastically at low temperature ($T < 0.5 T_m$, where T_m is the absolute melting temperature) have shown that the flow process can be practically described by steady state creep, which is controlled by grain boundary diffusion. These results indicated that the plastic flow takes place with a significant contribution of grain boundary sliding mechanism. Beside some attempts to show localization of plastic flow in the grain boundary regions,^{11,49–51)} there is a convincing direct experimental evidence for GBS by employing indentation and atomic force microscopy (AFM).^{11,51)}

Figure 2 shows an AFM image of the surface of an UFG pure Al sample deformed by Vickers indenter. There is a rumpling around the Vickers pattern, showing the displacement of grains relatively to each other in the UFG matrix. Careful analysis of the pile-ups formed around the Vickers patterns, observed by three-dimensional AFM measurements suggests that the contribution of the grain boundary sliding to the total strain in the ECAP-processed Al sample can reach up to 70%.¹¹⁾ This experiment demonstrates visibly the occurrence of intensive GBS, as a significant mechanism for plastic deformation (indentation) at room temperature in the ultrafine-grained Al.

We note here that in the case of pure Al, despite significant GBS, its ductility remains very poor at low temperatures, because the grain boundary diffusion is not fast enough to ensure that the material does not crack at the grain boundaries due to GBS. Intensive GBS controlled by fast grain boundary diffusion and its effect on ductility will be reviewed later, in section 3.

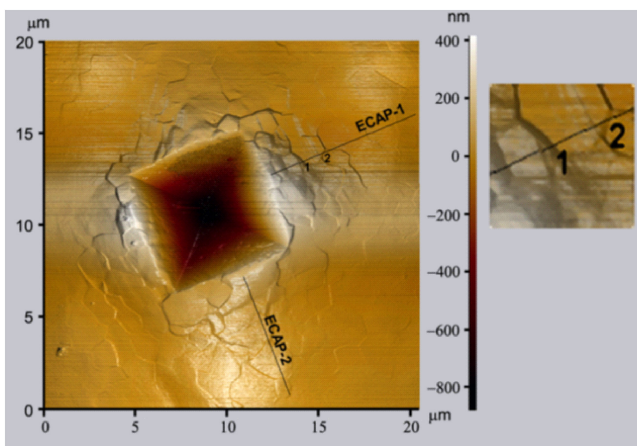


Fig. 2 Atomic force microscopy (AFM) image of the surface of an ultrafine-grained pure Al sample indented by a Vickers indenter. Reproduced with permission.⁵¹⁾ Copyright 2006, Elsevier.

2.3 The role of intensive GBS in the indentation size-effect in UFG metals

An important phenomenon during depth-sensing indentation is the so-called indentation size effect (ISE), referring to the scale dependent behavior of the hardness, namely that smaller indentation forces, and thus smaller indentation depths, are associated with higher hardness values. Due to this phenomenon, in many cases, when we want to compare the strength of certain materials, it is not enough to mention only the hardness of these materials, but it is also necessary to specify the conditions under which the hardness values were determined. So far, the origin of ISE is not yet fully understood, because many factors such as the friction along the indented surface,^{52,53)} imperfections in the indenter tip⁵⁴⁾ and/or the occurrence and effect of geometrically necessary dislocations (GNDs)⁵⁵⁾ may result in similar effect. Nevertheless, the latter is a widely accepted assumption that is very well suited to the interpretation of ISE for coarse-grained pure metals.

Recent experimental results,⁵⁶⁾ however, have shown that the ISE effect is not experienced at all in submicron Al and Cu having average grain size of about 100–120 nm. Mechanical properties of different composition Al–Cu layers having thickness of $\sim 1.7 \mu\text{m}$ were studied by using depth-sensing indentation. Figure 3 shows the hardness obtained on these layers at different maximum loads of 10, 20 and 50 mN. It can be seen that the hardness value obtained for both Al and Cu does not depend on the value of the maximum applied load, indicating that these submicron-grained pure metal samples are not sensitive to the indentation size effect. It is worth noting that these observations are in contrast to those described for conventional pure Al⁵²⁾ and Cu,⁵⁵⁾ where ISE is a known phenomenon.

The reason why no size effect is observed for the submicron-grained pure Al and Cu samples is the occurrence of intensive grain boundary sliding in these samples. As it has already been mentioned for pure Al, the analysis of the pile-ups formed around the Vickers patterns^{11,51,56)} led to the conclusion that the grain boundary sliding mechanism contributes at least 50–60% of the total deformation during

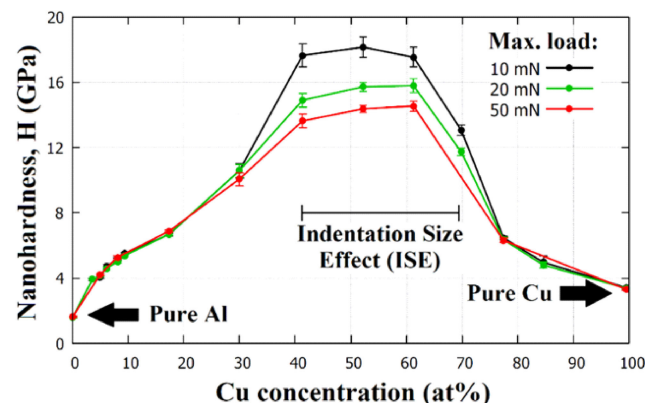


Fig. 3 Results of indentation tests, showing nanohardness values of pure Al and Al–Cu thin films over the whole range of Cu concentrations. The hardness values obtained at max. load of 10, 20 and 50 mN are plotted together to demonstrate the indentation size effect. Reproduced with permission.⁵⁶⁾ Copyright 2023, Elsevier.

indentation. Under these conditions, the effect of intra-grain dislocations, including geometrically necessary dislocations,⁵⁵⁾ is no longer significant due to intense grain boundary sliding. Therefore, the size effect cannot occur and cannot be observed.

We note that in the middle region of Fig. 3, where there is a high (40–70 at%) Cu content in the Al–Cu system, it can be seen that some samples show a strong size effect. These samples are also submicron-structured, but GBS is not significant in their plastic deformation. More details can be found in Ref. 56).

3. Effect of Grain Boundary Structure on Plastic Behaviors of UFG Al Alloys

3.1 Decomposition and wetted grain boundaries in HPT-processed Al–Zn alloys

Al–Zn alloys having different Zn content from 2 to 30 wt.% were processed by high-pressure torsion (HPT) to get UFG microstructures.^{57–59)} It is well established that together with significant grain-refinement, a decomposition of the microstructure was observed in the Al–Zn samples after HPT-processing up to 10 revolutions at RT. The initial grain size of about 60–70 μm has decreased to the final value lower than 1 μm and depended on the Zn content. The average grain sizes of Al–2 wt.% Zn, Al–5 wt.% Zn, Al–10 wt.% Zn and Al–30 wt.% Zn (denoted as Al–2Zn, Al–5Zn, Al–10Zn and Al–30Zn) alloys were about 950, 500, 435 and 350 nm, respectively.⁵⁹⁾

Microstructure of the HPT-processed Al–30Zn alloy can be seen in the transmission electron microscopy (TEM) images of Fig. 4. Together with the grain-refining effect (see Fig. 4(a)), HPT processing has also resulted in significant decomposition of the solid solution (Fig. 4(b)). The experimental observations of the HPT processed microstructure^{57–62)} have shown the formation of Zn particles in the Al/Al grain boundaries and mainly in grain boundary triple junctions and also inside the Al grains. The size and distribution of the Zn particles formed during HPT processing depend on the Zn content. In the case of the lowest Zn-concentrated Al–2Zn alloy, Zn particles with the size lower

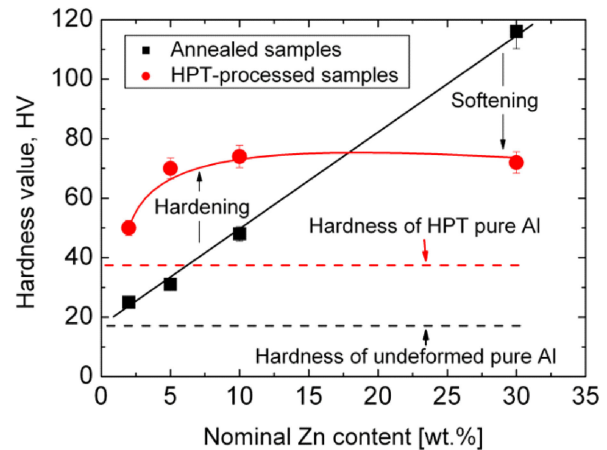


Fig. 5 Effect of high-pressure torsion processing on the hardness of Al–Zn alloys, illustrating both “normal” hardening and “abnormal” softening. Reproduced with permission.⁶³⁾ Copyright 2017, Elsevier.

than 20 nm can be found,⁵⁹⁾ but for the high Zn contents of 10 and 30 wt.%, larger particles of about 150–200 nm are formed in the triple junctions of the Al grains.

The decomposition of the initial solid solution (annealed) leads to significant change in mechanical properties of the HPT-processed alloys. Figure 5 shows the hardness of both the annealed and the HPT-processed, UFG Al–Zn alloys in the function of nominal Zn content.⁶³⁾ It can be clearly seen that for Zn concentrations not larger than 10 wt.%, the normal hardening-effect of SPD is observed, as the hardness of the HPT-processed samples is higher than that of the annealed samples. In contrast, there is a strong reduction in hardness of the high Zn-concentrated Al–30Zn alloy, indicating an abnormal softening due to HPT. As a result of SPD, the hardness of the UFG material does not increase, but decreases. The abnormal softening of the Al–30Zn alloy is certainly a consequence of the strong decomposition of the annealed microstructure in this alloy,⁶⁰⁾ as most of Zn solute atoms are then in the forms of Zn layers along Al/Al grain boundaries and Zn particles in triple junctions, resulting in a significant decrease in concentration and the strengthening effect of the (Zn) solute atoms in the matrix. Because of this, the hardness of the UFG sample is lower than that of the annealed counterpart.

Microstructural investigations^{59,60,64)} have also shown that together with the grain-refinement and the decomposition of the solid solution into Al matrix and Zn particles, the structure of grain boundaries in UFG samples is also changed significantly. Results obtained by using transmission electron microscopy and energy dispersive spectroscopy (EDS) have revealed clearly the presence of Zn-wetted grain boundaries, and therefore the segregation of Zn solute atoms into grain boundaries in high Zn-containing alloys.^{59,60,65)} In the case of high Zn-concentrated Al–30Zn sample, more than 50 percent of the Al/Al grain boundaries are wetted by Zn-rich layers as observed in Z-contrast high-angle annular dark field (HAADF) image and energy-dispersive X-ray spectroscopy (EDS) mapping of Fig. 6, as well as in the EDS line profile of Fig. 7. Both figures show well visibly that the concentration of Zn in grain boundary is much higher than that in the matrix.⁶⁰⁾ The high resolution transmission electron mi-

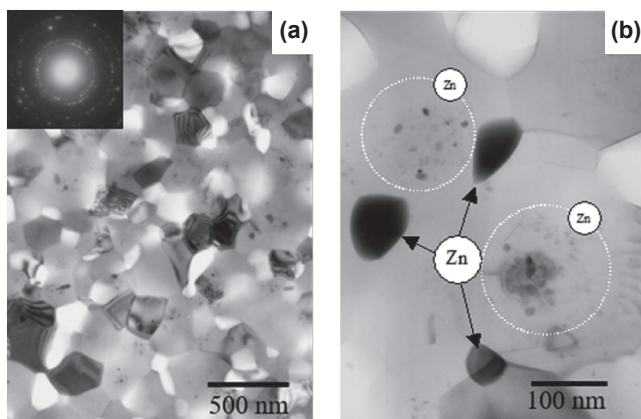


Fig. 4 TEM images on microstructure of the HPT-processed Al–30Zn sample, demonstrating (a) the UFG microstructure and (b) significant decomposition of the solid solution state. Reproduced with permission.⁵⁷⁾ Copyright 2010, Springer.

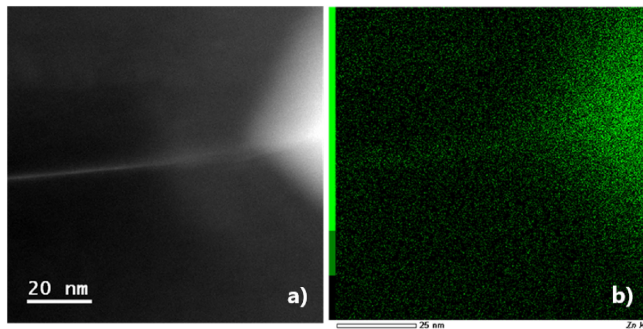


Fig. 6 High magnification TEM as (a) Z-contrast HAADF image showing a Zn particle on the right hand side and a brightly imaged grain boundary and (b) corresponding EDS map, confirming the high Zn concentration in the particle and the Zn grain boundary segregation. Reproduced with permission.⁶⁰⁾ Copyright 2014, Wiley.

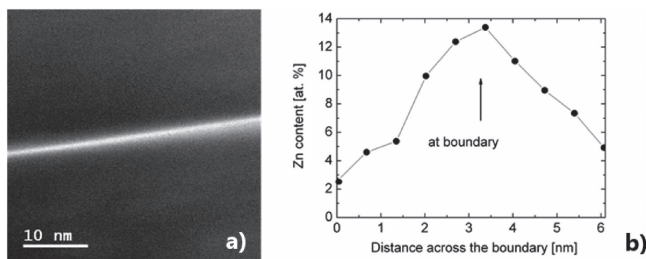


Fig. 7 High magnification TEM as (a) Z-contrast HAADF image showing Zn segregation along a grain boundary and (b) corresponding EDS line profile showing that the local Zn concentration along the boundary is higher than 10 at.% while it is in a range of 2 to 3 at.% in the Al matrix. Reproduced with permission.⁶⁰⁾ Copyright 2014, Wiley.

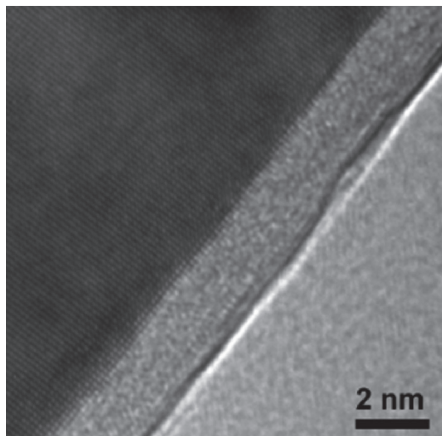


Fig. 8 High-resolution TEM image showing a wetting layer along an Al/Al grain boundary in the HPT-processed high Zn-concentrated Al-30Zn sample. Reproduced with permission.⁶⁴⁾ Copyright 2014, Elsevier.

croscopy (HRTEM) image of Fig. 8 shows a wetting layer having thickness of about 2 nm along an Al/Al grain boundary in the HPT-processed Al-30Zn sample.⁶⁴⁾ It should be noted that as the consequence of severe plastic deformation introduced by HPT, the decomposition of supersaturated solid solutions is often observed in other alloys, for instance, in Al-Mg⁶⁶⁾ and Cu-based alloys.⁶⁷⁾

3.2 Effect of wetted grain boundaries: unusually high strain rate sensitivity at RT

Looking at the mechanical properties, it is expected that

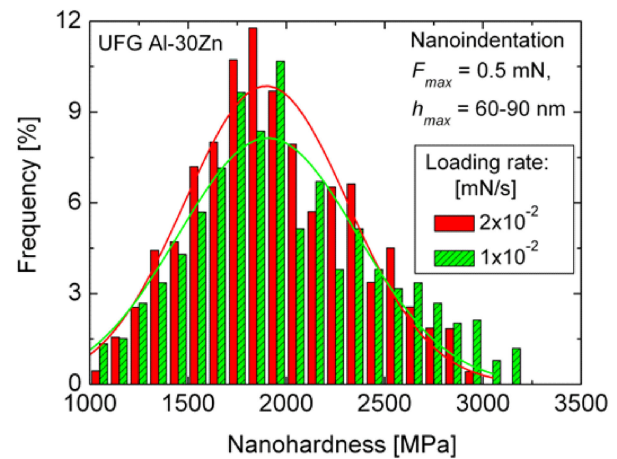


Fig. 9 Hardness-distribution obtained at the max. load of 0.5 mN for two different loading rates on UFG Al-30Zn alloy. The solid lines indicate Gaussian fit of the spectra, demonstrating the very low sensitivity to the loading rate. Reproduced with permission.⁶⁸⁾ Copyright 2012, Elsevier.

the presence of Zn-wetted grain boundaries significantly affects the behavior of the material. In order to study the possible role of the wetted grain boundaries in the UFG Al-30Zn alloy, nanoindentation measurements were made⁶⁸⁾ on both UFG Al-30Zn and UFG pure Al samples in different conditions to cause plastic deformation at different scales.

Considering the average grain size of about 350–400 nm for UFG Al-30Zn, in the first step a series of 400 nanoindentation measurements was made at a very low maximum load of 0.5 mN so that the size of the indentation pattern was about equal to the (400 nm) average grain size. In this case, the measurements were most probably carried out on individual grains in both UFG Al and Al-30Zn samples. Figure 9 shows the distribution of the hardness values obtained for two different loading rates on the UFG Al-30Zn sample. The experimental results have clearly revealed that these hardness-spectra are almost the same, indicating that when the deformation process takes place in small (about one grain) scale, the hardness-spectrum of UFG Al-30Zn is not sensitive to the loading rate, giving a low strain rate sensitivity (SRS).⁶⁸⁾

The application of higher maximum load of 1 mN results in larger size of the indentation pattern. In this case, the pattern-size was ~1–1.5 μm , which is about 3–4 times larger than the average grain size of the UFG Al-30Zn alloy, and therefore the Vickers pattern covers a group of at least ~5–7 grains during indentation. The corresponding experimental results presented in Fig. 10(a) clearly indicated that the hardness-distribution obtained on the UFG Al-30Zn alloy becomes sensitive to the loading rate when the deformation process takes place in larger scale, as in a group of several grains. Fitting Gaussian functions to the presented spectra and considering the peak value, a strain rate sensitivity of the UFG Al-30Zn alloy could be estimated, similarly to the results obtained by indentation creep method.⁶³⁾ These observations show clearly that, when a group of grains is plastically deformed in the UFG alloys, the role of the grain boundaries is enhanced and should be taken into account. The hardness spectra shown in Fig. 10(b) confirm the low strain rate sensitivity of UFG pure Al, as the hardness-

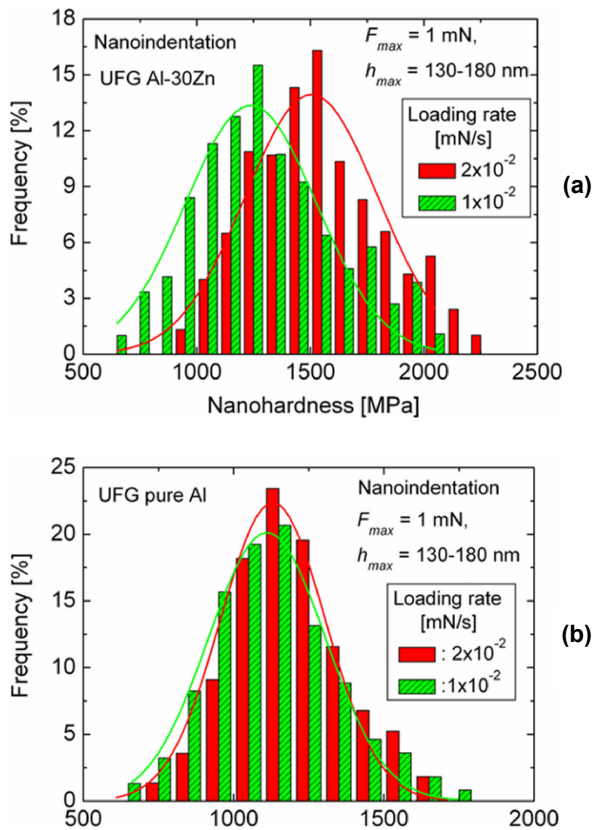


Fig. 10 Hardness-distribution obtained at the max. load of 1 mN for two different loading rates on (a) ultrafine-grained Al-30Zn alloy and (b) ultrafine-grained pure Al. The solid lines indicate the Gaussian fit of the spectra, demonstrating the higher sensitivity to the loading rate in the case of UFG Al-30Zn sample. Reproduced with permission.⁶⁸⁾ Copyright 2012, Elsevier.

distribution of this material is visibly insensitive to the loading rate.⁶⁸⁾

Recent experimental observations have also suggested a correlation between strain rate sensitivity and viscous behaviors of ultrafine-grained Al-Zn alloys.⁶⁹⁾ The strain rate sensitivity values obtained by using indentation creep⁷⁰⁾ on the HPT-processed Al-Zn samples are 0.08, 0.14, 0.17 and 0.25 for Al-2Zn, Al-5Zn, Al-10Zn and Al-30Zn, respectively,⁶³⁾ increasing with nominal Zn concentration and an unusually high value (0.25) was obtained for the high Zn-concentrated Al-30Zn alloy. In general, the ultrafine-grained materials produced by severe plastic deformation exhibit extremely low strain rate sensitivity of about 0.01–0.03.³⁶⁾ In the present case, the unusually high strain rate sensitivity should be attributed to the Zn addition. This is a consequence of the high fraction of Al/Al grain boundaries wetted by Zn-rich layers which lead to intensive grain boundary sliding (GBS) and then to a room temperature super-ductility of Al-30Zn sample,⁵⁷⁾ as shown in Fig. 11. The experimentally obtained tensile deformation curves presented in Fig. 11 indicate that both the stress and the total elongation of the UFG Al-30Zn sample depend strongly on the applied strain rate, even at room temperature. It can be seen that the ultrafine-grained Al-30Zn samples exhibit – together with unusually high strain rate sensitivity – unusually high ductility of about 160% when testing by tensile at room temperature.⁵⁷⁾

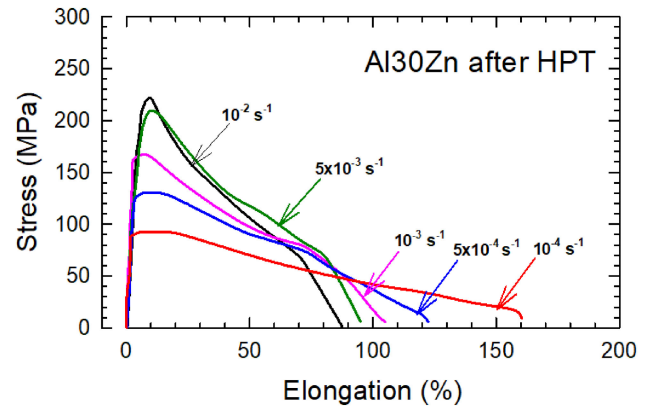


Fig. 11 Stress-strain curves of tensile deformation taken at different strain rates on UFG Al-30Zn samples, showing the room temperature super-ductility of this sample. Reproduced with permission.⁵⁷⁾ Copyright 2010, Springer.

The results suggest that Zn segregation at GBs significantly assisted GB slip, consequently achieving superplasticity in this UFG Al-Zn alloy. To understand the mechanism of segregated Zn grains supporting RT superplasticity and the evolution of Zn distribution during the whole superplastic deformation process, the authors studied specimens at different superplastic strains using the STEM-HAADF imaging technique at the nanoscale.⁶⁵⁾ The dynamic diffusion process of Zn is critical to RT superplasticity. At the early stages of deformation, Zn depleted zones are found close to the GBs, demonstrating an obvious segregation from the supersaturated grain matrix to the boundaries.⁶⁵⁾

Additionally, segregation also occurs in the matrix grains as evidenced by the formation of small Zn particles and bands, which may be related to the segregation of Zn to defect sites in the matrix and indicate a redistribution, leading to the nucleation of small Zn grains.⁶⁵⁾

With the increase of strain, the exhaustion of Zn lubricant is inevitable unless additional Zn atoms are supplied during the deformation process. Different from the early stages of deformation, when Zn is more concentrated at the center of grains at around 120% strain, Zn is rich at the vicinity of GBs, showing a grain-range Zn diffusion process. A high density of vacancies is usually required for diffusion over such a long range, which can be achieved by elevating the temperature. Alternatively, severe deformation processes, such as high-pressure torsion, can produce a similar vacancy density.⁶⁵⁾

The depletion of Zn at GBs is directly correlated with the end of superplastic deformation, that again highlights the importance of Zn to the observed superplasticity in this alloy.

The presence of a Zn nanolayer at GBs significantly reduces the energy barrier for GB sliding, confirming that the Zn nanolayer is an effective solid lubricant for GB sliding, resulting in the RT superplasticity observed in the experiments. All these results point to an important conclusion that continuous supply of Zn to GBs is critical to the RT superplasticity of the Al-Zn alloy.⁶⁵⁾

Significantly increasing the Zn content to 50 weight percent (in Al-30 at% Zn alloy),⁶²⁾ the effect of the wetted grain boundaries will be even more pronounced in the HPT-processed sample. It has been shown that in this case, the

plastic behavior of the HPT-processed Al–50Zn sample is characterized by even higher strain rate sensitivity of 0.4 and room temperature superplasticity over 400% tensile elongation. However, the strong Zn-wetted grain boundaries in this extra concentrated sample have enhanced grain boundary energy, which reduces the stability of grain boundaries. Because of this, the average grain size has significantly increased from 280 nm (before the tensile test) to 550 nm (after the test) during room temperature superplastic deformation. Furthermore, the natural aging – holding at room temperature – also causes changes in the microstructure and mechanical properties of the HPT-processed sample.⁶²⁾

3.3 Enhancing effect of segregated GBs on GB diffusion

It has been shown that the intensive GBS in the system having Zn-wetted grain boundaries is controlled by relatively high diffusion of Zn atoms along grain boundary.⁶⁸⁾ Performing hardness measurements at different temperatures, the activation energy of 65 kJ/mole characterizing the deformation process in the ultrafine-grained Al–30Zn alloy was obtained experimentally.⁶⁸⁾ This activation energy is lower than the values for self-diffusion in Al (142 kJ/mole¹⁸⁾), self-diffusion in Zn (92 kJ/mole¹⁸⁾) or that for grain boundary diffusion in Al (84 kJ/mole¹⁸⁾), suggesting that the process of plastic deformation of UFG Al–30Zn is controlled neither by the self-diffusion of Al nor the self-diffusion of Zn atoms. Based on low activation energy and some reasonable parameters,⁶⁸⁾ a relatively high diffusivity ($\sim 10^{-15} \text{ m}^2 \text{ s}^{-1}$) value has been estimated for the room temperature diffusion coefficient in the UFG Al–30Zn alloy. Considering the fact that this value is correlating with the measured, relatively high diffusivity for Zn diffusion along Al/Al grain boundaries,^{71,72)} it has been suggested that the process of plastic deformation in UFG Al–30Zn alloy at room temperature is controlled by Zn diffusion along the Al/Al grain boundaries. This finding emphasizes the importance of the Zn-rich layers covering Al/Al boundaries in the ultrafine-grained Al–Zn alloys. The accelerated diffusion of Zn along the Al/Al boundaries do certainly enhance the development of grain boundary sliding. This situation is similar to that in the case of the Zn–22%Al eutectoid alloy processed by SPD,⁷³⁾ where the fraction of Al/Al boundaries plays a critical role in GBS mechanism.

Diffusion of atoms in a supersaturated solid solution during aging at relatively high temperatures can also lead to the formation of GP zones in Al alloys including Al–Zn alloys.^{74,75)} GP zones are regions enriched with alloying elements and usually present distinct shapes and boundaries with a diameter of a few nanometres.^{76,77)} Chemical ordering has also been reported in GP zones.^{78,79)}

It has been widely recognised that chemical short-range order (SRO) is an important factor that determines deformation mechanism, consequently impacting mechanical properties,^{80,81)} the SRO effect on unusual mechanical behaviours of ultrafine-grained Al–Zn alloys (such as room-temperature superplasticity) is demonstrated, which deserves detailed future studies. In summary, clusters with chemical SRO and dimensions of 1–3 nm were found in a severely deformed supersaturated Al–30Zn alloy. Structural characterisation and DFT calculations suggested that the ordered phase

is of the L10 structure. The severe tensile deformation with strain of 150% introduces a high density of vacancies, enabling short-range atomic diffusion and re-arrangement to achieve a low-energy ordered structure at room temperature.

Considering both the fast diffusion and the unusually high strain rate sensitivity, significant grain boundary sliding could also be predicted in the ultrafine-grained Al–Zn alloys. These factors together lead to the super-ductility⁵⁷⁾ and even superplasticity⁶²⁾ of these UFG alloys at room temperature. It should be mentioned that intensive grain boundary sliding is quite typical for the deformation of UFG metal materials, but it is usually not accompanied by high SRS and does not lead to high formability if the grain boundary diffusion is not fast enough. A typical such case is the pure UFG Al described in point 2.2. In the present case, the fast diffusion and high SRS are also characteristics of the UFG material. Both intensive GBS and the correlation between strain rate sensitivity and ductility of UFG Al–30Zn have been proved by deforming micro-pillars.⁶⁰⁾ In these experiments, micro-pillars having diameters of $\sim 3 \mu\text{m}$ and heights of $\sim 10 \mu\text{m}$ were fabricated on the surface of HPT-processed UFG sample, and also on the surface of initial (annealed) samples and then they were deformed by nanocompression.⁶⁰⁾

It should be noted that for these compression tests, the pillars prepared on the surface of the HPT-processed Al–30Zn sample having a grain size of $\sim 300\text{--}400 \text{ nm}$ can be regarded as polycrystalline specimens. In contrast, the pillars in the annealed, coarse-grained conventional samples, are rather single crystals.

Figure 12 shows some typical stress-strain curves obtained on the compressed pillars. There is a significant difference between the deformation processes of the two types of pillars. First of all, it can be seen that the flow stresses of the conventional samples are much higher than that of the HPT-processed UFG samples, again demonstrating the abnormal softening of the HPT-processed sample, mentioned before, in section 3.1. Further significant differences can be observed

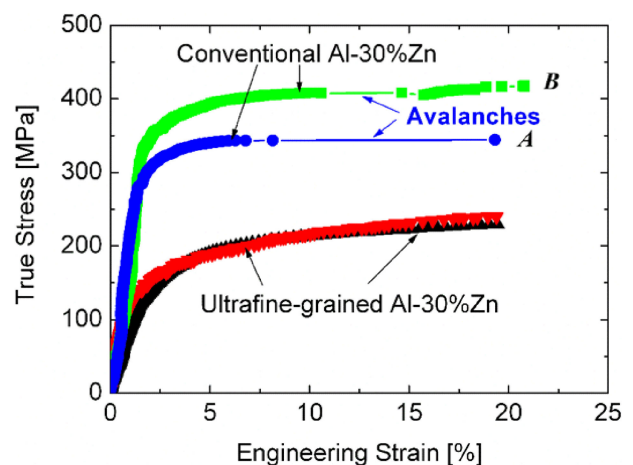


Fig. 12 Typical stress-strain curves obtained for micro-pillars on the surface of coarse-grained (conventional) and HPT-processed ultrafine-grained Al–30Zn samples, showing strain avalanches in the single crystal pillars on the conventional sample, and smoothly stable deformation without avalanches in the ultrafine-grained pillars. The single crystal pillars A and B have orientations near $\langle 100 \rangle$ and $\langle 111 \rangle$, respectively. Reproduced with permission.⁶⁰⁾ Copyright 2014, Wiley.

between the deformation behaviors of the conventional coarse-grained and ultrafine-grained samples. It can be observed that strong strain avalanches occurred during compression, and because of this, the development of the deformation curves is not continuous. In contrast, the stress-strain curves obtained for the ultrafine-grained pillar-samples are smooth with a marked absence of any strain avalanches.⁶⁰⁾

The phenomenon of deformation localization as strain avalanches is well-known for the plasticity of small-size – micrometer-scale – single crystals.^{12,13,82–85)} In the case of the ultrafine-grained pillars, which are polycrystalline samples, however, the role of the grain boundaries may be very significant. Therefore, when discussing the plastic behaviors of the UFG micro-pillars, the effect of grain boundaries must be taken into account. Considering the Hall-Petch relationship, grain boundaries can act as obstacles against moving dislocations, and at the same time themselves can become a source for dislocations. Furthermore, in the case of special structure, as wetted grain boundaries, grain boundary diffusion can be accelerated, leading to the occurrence of significant grain boundary sliding. In this case, the deformation process will take place primarily through the motion of grain boundaries. Considering these compensating effects, it can be concluded that strain avalanches will not take place in the polycrystalline pillars. The smooth flow of the ultrafine-grained pillars should be attributed to the effect of the grain boundaries.

The investigation of the deformed pillars by scanning electron microscopy (SEM) have also shown significant differences between the deformation mechanism of the conventional coarse-grained and ultrafine-grained samples. Typical surface morphologies of these samples can be seen in the SEM images of Fig. 13. In the case of the conventional coarse-grained pillar (see Figs. 13(a) and 13(b)) deformation localizations and extreme slip bands can be observed near to the direction of maximum shear stress at 45° relative to the orientation of the compression stress. In contrast, no deformation localizations and extreme slip bands are observed on the surface of the deformed ultrafine-grained pillars as demonstrated in Figs. 13(c) and 13(d) in different magnifications.

3.4 Unique effect of grain boundary segregation: Superplasticity at extremely low temperature in commercial UFG 7xxx Al alloy

Considering again eq. (4), it has already been mentioned in section 2.2 that a decrease of grain size should improve the occurrence of steady state flow, even the occurrence of superplastic process at relatively low temperatures.

It is well known that the main deformation mechanism of superplastic deformation is diffusion-controlled grain boundary sliding.^{86,87)} In the case of conventional superplastic materials^{43,88,89)} having grain size of about 5–10 μm , relatively high testing temperature at $\sim 0.7\text{--}0.8 T_m$, where T_m is the absolute melting temperature of the material, is required to ensure continuous grain boundary diffusion. Experimental results have shown that when the average grain size is decreasing into the range of submicron, the temperature necessary for the occurrence of superplasticity is significantly decreasing. Several ultrafine-grained

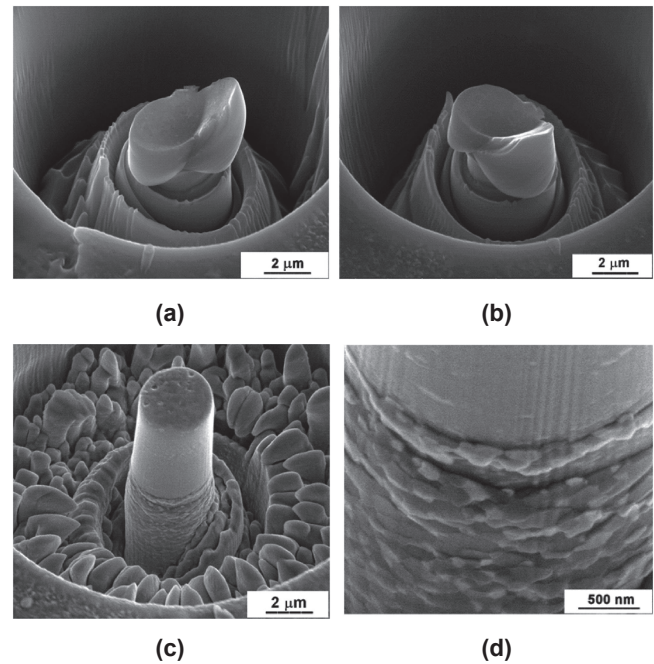


Fig. 13 Surface morphologies of the compressed pillars on the surface of (a)–(b) the coarse-grained Al–30Zn sample (sample A in Fig. 12) in two different positions (separated by 60° rotation), showing strain localizations and extreme slip bands and (c)–(d) the HPT-processed ultrafine-grained Al–30Zn sample at low and high magnifications, respectively, demonstrating a direct evidence for the occurrence of intensive GBS without any deformation localization. Reproduced with permission.⁶⁰⁾ Copyright 2014, Wiley.

AlMg-,^{90–96)} AlLi-^{91,97)} and 7xxx AlZnMg-based^{91,98,99)} samples have shown superplastic behaviors in the low temperature range between $0.5\text{--}0.7 T_m$.

Regarding superplastic deformation, it should be noted that GBS is an important factor, but it is not enough for a material to be deformed superplastically. The GBS must be maintained continuously by adequate grain boundary diffusion, otherwise a boundary crack will form and lead to rapid fracture. At low temperatures, it is not easy to provide a sufficiently fast diffusion, and therefore it is difficult to achieve superplasticity at temperatures lower than $0.5 T_m$. Recently,¹⁰⁰⁾ new grain boundary approach was investigated and demonstrated for an Al–Zn–Mg–Zr alloy, which is one of the basic materials in the aluminum industry. It was found that the process of grain boundary diffusion could be enhanced in the UFG alloy having unique grain boundary behaviors controlled by grain boundary segregation, leading to superplasticity with a record total elongation at temperature lower than $0.5 T_m$.

The alloy with a composition of Al–4.8 wt.%Zn–1.2 wt.%Mg–0.14 wt.%Zr was ultrafine-grained by HPT. As a result of HPT, a saturated UFG microstructure having average grain size of 200 nm was produced. It has also been shown that this UFG structure is relatively stable under 200°C ($0.5 T_m$), as the average grain size was practically unchanged after annealing at 120°C for 2 h, and it increased only to about 300 nm at 170°C.¹⁰¹⁾ Furthermore, unusually high strain rate sensitivity of $\sim 0.40\text{--}0.43$ was obtained in this temperature region, indicating that superplasticity can be expected at low temperatures. Figure 14 shows the typical

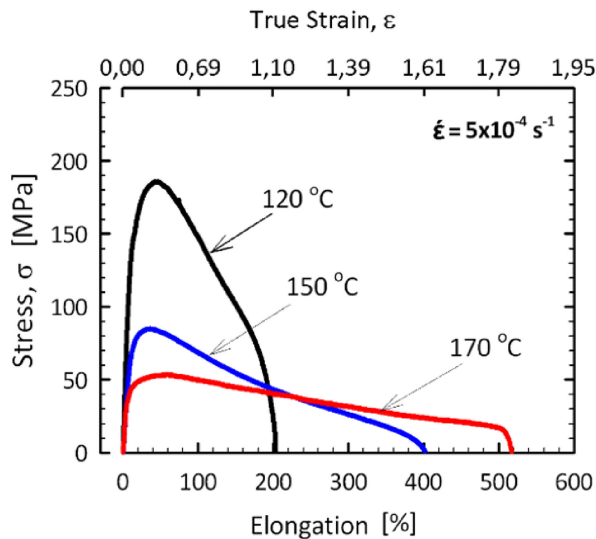


Fig. 14 Deformation curves of the UFG Al-Zn-Mg-Zr alloy, showing a total elongation higher than 500% at 170°C (0.47 homologous temperature). Reproduced with permission.¹⁰⁰⁾ Copyright 2021, Taylor & Francis.

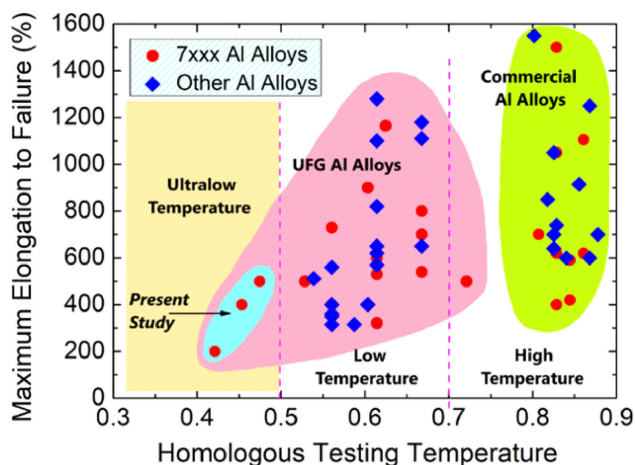


Fig. 15 Significance of ultralow-temperature superplasticity in the UFG Al-Zn-Mg-Zr alloy (denoted as Present Study) indicated by reviewing the temperature dependence of superplasticity of commercial Al alloys of 7000 (AlZnMg-based) system^{91,98,99,102–109)} and other (AlMg-, AlLi-based) systems.^{90–97)} Reproduced with permission.¹⁰⁰⁾ Copyright 2021, Taylor & Francis.

stress-strain curves of superplastic deformation taken at strain rate, $\dot{\epsilon}$ of $5 \times 10^{-4} \text{ s}^{-1}$ at 120, 150 and 170°C. It can be seen that the total elongation of almost 200% is obtained at very low temperature of 120°C, and a record deformation higher than 500% was observed at 170°C (0.47 T_m).

Considering the superplasticity of commercial Al alloys, the summary graph in Fig. 15 shows the significance of the mentioned new results obtained on the UFG AlZnMg alloy.¹⁰⁰⁾ It can be seen that conventional commercial Al alloys, having average grain-size of 1–10 μm , can typically be superplastically deformed in the high (>0.7) homologous testing temperature range.^{92,102–109)} Ultrafine-grained Al alloys with lower average grain-size of 100–700 nm show superplastic behavior mainly in the low homologous temperature region between 0.5 and 0.7.^{90–99)} For lower homologous temperature, in the ultralow region under 0.5,

there are only data from the mentioned research¹⁰⁰⁾ with the total elongation of 500% at homologous temperature of 0.47.

The record low-temperature superplasticity is due to the fact that the activation energy characteristic of grain boundary diffusion is relatively small. Therefore, even at low temperatures, relatively fast diffusion can be ensured during grain boundary sliding. Calculations¹⁰⁰⁾ have showed that the diffusion coefficient characteristic of the grain boundary sliding of the mentioned UFG AlZnMg alloy at 170°C is almost two orders of magnitude higher than the aforementioned value calculated for grain boundary diffusion in pure Al. This fast diffusion is the consequence of unique structure of grain boundaries in the UFG material. Figure 16 shows a typical HAADF image with the corresponding EDS maps and EDS line profile on the grain boundary structure in the sample deformed superplastically for a total elongation higher than 500% at 170°C. The EDS results reveal clearly the depletion of Al, as well as the excess of Mg and Zn atoms in the Al/Al grain boundaries of this HPT-processed UFG sample. The matrix grain boundaries of this UFG sample can be regarded as Zn/Mg-rich boundaries. For instance, according to Fig. 16(e), this sum of Zn and Mg concentrations in the boundary reached about 10 at%. As mentioned in Section 3.1, the strong segregation of Zn to the matrix grain boundaries is already a known phenomenon in high-Zn concentrated model binary Al-Zn alloys with a UFG structure, but it has not been reported yet for the 7xxx series Al alloys. It should also be noted that the segregation of solute atoms into grain boundaries due to HPT processing was recently confirmed by numerical and analytical calculations.¹¹⁰⁾ This kind of segregation is a key point in the observed ultralow-temperature superplasticity for the UFG Al-Zn-Mg-Zr alloy.¹⁰⁰⁾

4. Innovation Potential of Unique Grain Boundary Phenomenon

4.1 Advantage of intensive GBS at RT for micro-devices

Considering the deformation processes occurring at RT in the coarse-grained and ultrafine-grained Al-30Zn micro-pillars shown in Figs. 12 and 13, it is clear that the strain localizations and extreme slip bands observed in the coarse-grained samples (Figs. 13(a) and 13(b)) correlate directly with the strain avalanches visible in the compression curves of the coarse-grained micro-pillars. As the large strain fluctuations may lead to uncertainties in plastically forming micrometer-scale single crystals,¹²⁾ micrometer-sized samples of coarse-grained metals are not suitable for use in the fabrication of micro-devices, in practical applications.

By contrast, consistent with the smoothly stable deformation process (see in Fig. 12), no strain localizations or extreme slip bands can be observed in the deformed UFG micro-pillars as shown in Figs. 13(c) and 13(d). The observed surface morphologies provide a very clear demonstration of the occurrence of intensive GBS in the plastic deformation of the ultrafine-grained pillars. The stable deformation by intensive grain boundary sliding at room temperature of the UFG micro-pillars – without the occurrence of any catastrophic avalanches – emphasizes the significance of the sliding mechanism, suggesting an

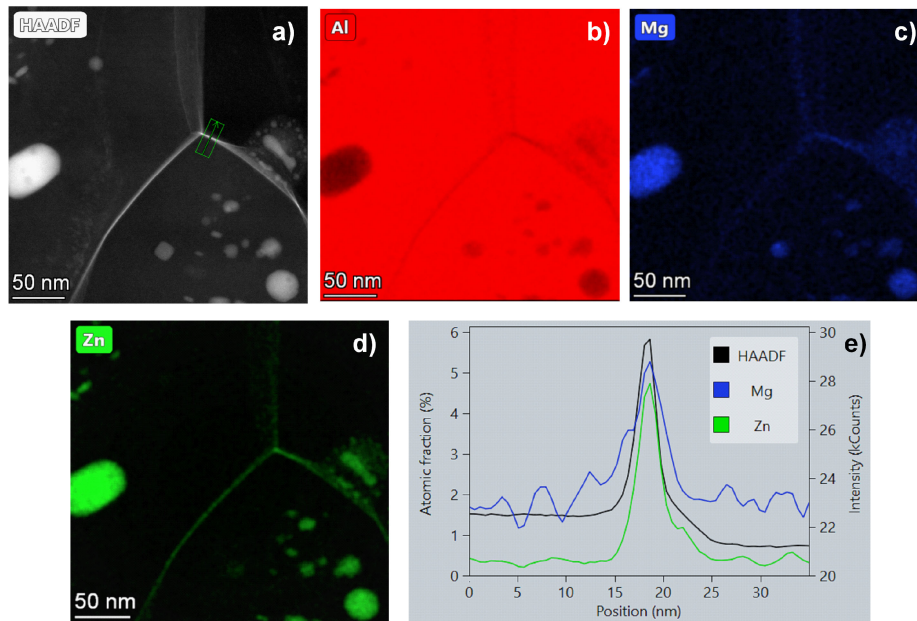


Fig. 16 Grain boundaries in the AlZnMg sample superplastically deformed at 170°C: (a) High magnification HAADF image showing Zn-rich grain boundaries (forming a brightly imaged triple junction). (b)–(d) corresponding EDS maps for Al, Mg and Zn, respectively. (e) EDS line profile analysis along a boundary, marked by arrows in the HAADF image, showing the segregation of Zn and Mg atoms into Al/Al grain boundaries in the HPT-processed UFG sample. Reproduced with permission.¹⁰⁰⁾ Copyright 2021, Taylor & Francis.

important potential for using the UFG materials in the fabrication of micro-devices.

4.2 Combination of high strength and low-temperature superplasticity in commercial Al alloys

It is well known that superplasticity of commercial Al alloys is an important field of materials science from the viewpoint of both basic and applied researches.

Considering again the Hall-Petch effect, the significant advantage of low-temperature superplasticity is, on the one hand, the potential energy savings during low temperature deformation, and on the other hand, the preservation of the fine-grained microstructure. Experimental results¹⁰⁰⁾ have shown that, the AlZnMg sample after superplastic deformation at 170°C remains equiaxial and ultrafine-grained with an average grain size of about 400 nm. Furthermore, MgZn₂ phase small precipitates having size between 10 and 70 nm were formed inside the grains during superplastic deformation. As consequence of the strengthening effect of both the UFG structure and the precipitates, the material retains its high strength even after superplastic deformation, as shown in Fig. 17, where the room temperature hardness of the HPT-processed and the superplastically deformed UFG samples can be seen and compared with the peak hardness of the initial coarse-grained sample.¹⁰⁰⁾ It can be seen that the hardness values of the samples after superplastic deformation (1280 and 1560 MPa at 170 and 120°C, respectively) are still 20–50% higher than the mentioned peak hardness of the initial (coarse-grained) sample after the so-called conventional T6 treatment,^{111,112)} which is an often-used heat treatment for 7xxx series alloys to get maximum strength.

More innovative applications of other UFG materials can be found elsewhere.¹¹³⁾

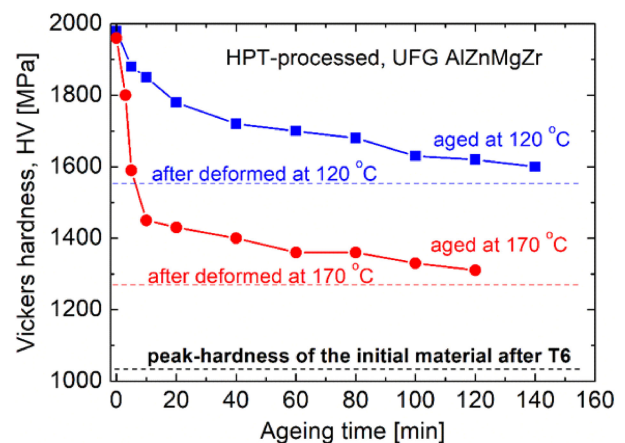


Fig. 17 Room temperature Vickers hardness of the HPT-processed, UFG AlZnMgZr samples after superplastic deformation at 120°C (blue dashed line) and 170°C (red dashed line), as well as the peak hardness obtained for the initial sample after the conventional T6 treatment (black dashed line). The hardness values of the UFG samples statically annealed for different times at 120°C (blue solid square) and 170°C (red solid circle) are also plotted to show the thermal stability of the sample. Reproduced with permission.¹⁰⁰⁾ Copyright 2021, Taylor & Francis.

5. Summary

The effect of grain size and grain boundaries on unusual mechanical and plastic behaviors of ultrafine-grained Al and Al alloys are reviewed. The main points of the review are the followings:

- (1) An appropriate modification of the original Hall-Petch equation has been suggested in order to keep its applicability for submicron-structured Al and other face-centered cubic (fcc) metals, as well as for their solid solution alloys. The modified Hall-Petch equation

allows us to estimate the strength of any sub-micron structured fcc metal or solid solution when the grain-size is known.

- (2) Experimental evidences have been shown which suggest that deformation by grain boundary sliding is especially favored in submicron structured materials. Depending on the structure of the grain boundary, grain boundary sliding can be associated with high strain rate sensitivity, which can lead to superductility, or even to superplasticity of the material.
- (3) As a consequence of the intensive grain boundary sliding, the indentation size effect well known for conventional coarse-grained materials does not occur in the case of submicron-structured materials.
- (4) It has been shown that an abnormal softening has occurred due to microstructural decomposition in the case of model UFG Al–Zn alloys processed by high-pressure torsion. Furthermore, the strong microstructure decomposition in high Zn-concentrated alloy leads also to the formation of Zn-rich grain boundary layers, which wet the Al/Al grain boundaries and enhance the role of grain boundary sliding in plasticity with an unusually high strain rate sensitivity. The same phenomenon was observed due to the grain boundary segregation of Zn solutes in a commercial UFG AlZnMg alloy.
- (5) The presented results demonstrate the significance of an enhancement in diffusion along the grain boundaries which promotes flow by grain boundary sliding. The occurrence of intensive GBS leads to a room temperature super-ductility of UFG Al–Zn alloys, and to the record superplasticity of the commercial UFG AlZnMg alloy.
- (6) Due to the significant role of grain boundaries in plasticity of UFG materials, the deformation process is relatively homogenous and stable at the micro-scale without the detrimental strain avalanches. Engineering of the microstructure, for example by solute segregations along the grain boundaries, makes it possible to achieve superplasticity at low temperatures, even at room temperature, and this effect may have important practical implications in electronic industry and especially for using these materials in micro-devices.
- (7) The presented results also demonstrate the possibility of extremely low-temperature superplasticity in traditional commercial Al alloys of the 7xxx series. The discovery of the low-temperature superplasticity creates an opportunity for the development of new technologies for the superplastic forming of complex-shaped products exhibiting a high structural strength in operating conditions at room temperature.

Acknowledgments

This work was supported by the KDP-2021 Program of the Ministry of Innovation and Technology from the source of the National Research, Development and Innovation Fund. Research of NQC, DO was also supported by the Hungarian-Russian Research program (TÉT) No. 2021-1.2.5-TÉT-IPARI-RU-2021-00001. Support from Hungarian Scientific

Research Fund OTKA, Grant number K143216 is also greatly acknowledged. The work of RZV and EVB was supported by the Ministry of Science and Higher Education of the Russian Federation under project No. 13.2251.21.0196 (grant agreement No. 075-15-2023-443).

REFERENCES

- 1) R.Z. Valiev, R.K. Islamgaliev and I.V. Alexandrov: *Prog. Mater. Sci.* **45** (2000) 103–189.
- 2) T.G. Langdon: *Mater. Sci. Eng. A* **462** (2007) 3–11.
- 3) R.Z. Valiev and T.G. Langdon: *Prog. Mater. Sci.* **51** (2006) 881–981.
- 4) T.G. Langdon: *Acta Mater.* **61** (2013) 7035–7059.
- 5) K. Edalati and Z. Horita: *Mater. Sci. Eng. A* **652** (2016) 325–352.
- 6) N. Kamikawa, N. Tsuji, X. Huang and N. Hansen: *Acta Mater.* **54** (2006) 3055–3066.
- 7) N. Kamikawa, X. Huang, N. Tsuji and N. Hansen: *Acta Mater.* **57** (2009) 4198–4208.
- 8) X. Huang, N. Hansen and N. Tsuji: *Science* **312** (2006) 249–251.
- 9) Y.T. Zhu, R.Z. Valiev, T.G. Langdon, N. Tsuji and K. Lu: *MRS Bull.* **35** (2010) 977–981.
- 10) G. Faraji and H. Torabzadeh: *Mater. Trans.* **60** (2019) 1316–1330.
- 11) N.Q. Chinh, P. Szommer, Z. Horita and T.G. Langdon: *Adv. Mater.* **18** (2006) 34–39.
- 12) D.M. Dimiduk, C. Woodward, R. LeSar and M.D. Uchic: *Science* **312** (2006) 1188–1190.
- 13) P.D. Ispánovity, Á. Hegyi, I. Groma, G. Györgyi, K. Ratter and D. Weygand: *Acta Mater.* **61** (2013) 6234–6245.
- 14) E. Voce: *J. Inst. Met.* **74** (1948) 537–562.
- 15) A.H. Cottrell: *Dislocations and Plastic Flow in Crystals*, (Clarendon Press, Oxford, 1953).
- 16) E.O. Hall: *Proc. Phys. Soc. B* **64** (1951) 747–753.
- 17) N.J. Petch: *J. Iron Steel Inst.* **174** (1953) 25–28.
- 18) H.J. Frost and M.F. Ashby: *Deformation-Mechanism Maps: The Plasticity and Creep of Metals and Ceramics*, (Pergamon Press, Oxford, 1982).
- 19) X.L. Wu, J. Narayan and Y.T. Zhu: *Appl. Phys. Lett.* **93** (2008) 031910.
- 20) E.O. Hall: *Nature* **173** (1954) 948–949.
- 21) R.Z. Valiev, Y. Estrin, Z. Horita, T.G. Langdon, M. Zehetbauer and Y.T. Zhu: *JOM* **58**(4) (2006) 33–39.
- 22) X. Sauvage, A. Duchaussoy and G. Zaher: *Mater. Trans.* **60** (2019) 1151–1158.
- 23) R.Z. Valiev, B. Straumal and T.G. Langdon: *Annu. Rev. Mater. Res.* **52** (2022) 357–382.
- 24) R.Z. Valiev: *Nat. Mater.* **3** (2004) 511–516.
- 25) R.B. Figueiredo and T.G. Langdon: *J. Mater. Res. Technol.* **14** (2021) 137–159.
- 26) F.A. Mohamed and Y. Xun: *Mater. Sci. Eng. A* **354** (2003) 133–139.
- 27) J. Gubicza, N.Q. Chinh, J.L. Lábár, Z. Hegedűs, P. Szommer, G. Tichy and T.G. Langdon: *J. Mater. Sci.* **43** (2008) 5672–5676.
- 28) N.Q. Chinh, J. Gubicza, T. Czeppe, J. Lendvai, C. Xu, R.Z. Valiev and T.G. Langdon: *Mater. Sci. Eng. A* **516** (2009) 248–252.
- 29) Y. Ito, K. Edalati and Z. Horita: *Mater. Sci. Eng. A* **679** (2017) 428–434.
- 30) S. Dangwal, K. Edalati, R.Z. Valiev and T.G. Langdon: *Crystals* **13** (2023) 413.
- 31) A. Mohammadi, N.A. Enikeev, M.Y. Murashkin, M. Arita and K. Edalati: *J. Mater. Sci. Technol.* **91** (2021) 78–89.
- 32) Y. Chen, N. Gao, G. Sha, S.P. Ringer and M.J. Starink: *Acta Mater.* **109** (2016) 202–212.
- 33) P.V. Liddicoat, X.Z. Liao, Y. Zhao, Y.T. Zhu, M.Y. Murashkin, E.J. Lavernia, R.Z. Valiev and S.P. Ringer: *Nat. Commun.* **1** (2010) 63.
- 34) J.R. Weertman: *Mater. Sci. Eng. A* **166** (1993) 161–167.
- 35) M. Furukawa, Z. Horita, M. Nemoto, R.Z. Valiev and T.G. Langdon: *Acta Metall.* **44** (1996) 4619–4629.
- 36) M.A. Meyers, A. Mishra and D.J. Benson: *JOM* **58**(4) (2006) 41–48.
- 37) C.Y. Yu, P.W. Kao and C.P. Chang: *Acta Mater.* **53** (2005) 4019–4028.
- 38) N. Kamikawa, T. Hirooka and T. Furuha: *Mater. Sci. Technol.* **37** (2021) 210–223.

- 39) H. Zhang, F. Liu, G. Ungar, Z. Zheng, Q. Sun and Y. Han: *Commun. Phys.* **5** (2022) 329.
- 40) N.Q. Chinh, D. Olasz, A.Q. Ahmed, G. Sáfrán, J. Lendvai and T.G. Langdon: *Mater. Sci. Eng. A* **862** (2023) 144419.
- 41) J.W. Edington, K.N. Melton and C.P. Cutler: *Prog. Mater. Sci.* **21** (1976) 61–170.
- 42) T.G. Langdon: *Acta Metall. Mater.* **42** (1994) 2437–2443.
- 43) T.G. Nieh, J. Wadsworth and O.D. Sherby: *Superplasticity in Metals and Ceramics*, (Cambridge University Press, Cambridge, 1997).
- 44) N.Q. Chinh, P. Szommer, J. Gubicza, M. El-Tahawy, E.V. Bobruk, M.Y. Murashkin and R.Z. Valiev: *Adv. Eng. Mater.* **22** (2020) 1900672.
- 45) N.Q. Chinh, G. Horváth, Z. Horita and T.G. Langdon: *Acta Mater.* **52** (2004) 3555–3563.
- 46) Y.M. Wang and E. Ma: *Mater. Sci. Eng. A* **375–377** (2004) 46–52.
- 47) N.Q. Chinh, J. Illy, Z. Horita and T.G. Langdon: *Mater. Sci. Eng. A* **410–411** (2005) 234–238.
- 48) N.Q. Chinh, T. Csanádi, J. Gubicza and T.G. Langdon: *Acta Mater.* **58** (2010) 5015–5021.
- 49) A. Vinogradov, S. Hashimoto, V. Patlan and K. Kitagawa: *Mater. Sci. Eng. A* **319–321** (2001) 862–866.
- 50) C.Y. Yu, P.L. Sun, P.W. Kao and C.P. Chang: *Scr. Mater.* **52** (2005) 359–363.
- 51) N.Q. Chinh, P. Szommer, T. Csanádi and T.G. Langdon: *Mater. Sci. Eng. A* **434** (2006) 326–334.
- 52) M. Atkinson: *J. Mater. Res.* **10** (1995) 2908–2915.
- 53) N.Q. Chinh, J. Gubicza, Zs. Kovács and J. Lendvai: *J. Mater. Res.* **19** (2004) 31–45.
- 54) J. Menčík and M.V. Swain: *J. Mater. Res.* **10** (1995) 1491–1501.
- 55) W.D. Nix and H. Gao: *J. Mech. Phys. Solids* **46** (1998) 411–425.
- 56) D. Olasz, G. Sáfrán, N. Szász, G. Huhn and N.Q. Chinh: *Mater. Lett.* **330** (2023) 133409.
- 57) R.Z. Valiev, M.Yu. Murashkin, A. Kilmametov, B.B. Straumal, N.Q. Chinh and T.G. Langdon: *J. Mater. Sci.* **45** (2010) 4718–4724.
- 58) E.V. Bobruk, X. Sauvage, N.A. Enikeev, B.B. Straumal and R.Z. Valiev: *Rev. Adv. Mater. Sci.* **43** (2015) 45–51.
- 59) X. Sauvage, M.Yu. Murashkin, B.B. Straumal, E.V. Bobruk and R.Z. Valiev: *Adv. Eng. Mater.* **17** (2015) 1821–1827.
- 60) N.Q. Chinh, R.Z. Valiev, X. Sauvage, G. Varga, K. Havancsák, M. Kawasaki, B.B. Straumal and T.G. Langdon: *Adv. Eng. Mater.* **16** (2014) 1000–1009.
- 61) A. Alhamidi, K. Edalati, Z. Horita, S. Hirose, K. Matsuda and D. Terada: *Mater. Sci. Eng. A* **610** (2014) 17–27.
- 62) K. Edalati, Z. Horita and R.Z. Valiev: *Sci. Rep.* **8** (2018) 6740.
- 63) N.Q. Chinh, P. Jenei, J. Gubicza, E.V. Bobruk and R.Z. Valiev: *Mater. Lett.* **186** (2017) 334–337.
- 64) B.B. Straumal, X. Sauvage, B. Baretzky, A.A. Mazilkin and R.Z. Valiev: *Scr. Mater.* **70** (2014) 59–62.
- 65) Z. Song, R. Niu, X. Cui, E.V. Bobruk, M.Yu. Murashkin, N.A. Enikeev, J. Gu, M. Song, V. Bhatia, S.P. Ringer, R.Z. Valiev and X. Liao: *Acta Mater.* **246** (2023) 118671.
- 66) B.B. Straumal, B. Baretzky, A.A. Mazilkin, F. Philipp, O.A. Kogtenkova, M.N. Volkov and R.Z. Valiev: *Acta Mater.* **52** (2004) 4469–4478.
- 67) B.B. Straumal, A.R. Kilmametov, Y. Ivanisenko, L. Kurmanaeva, B. Baretzky, Y.O. Kucheev, P. Zieba, A. Korneva and D.A. Molodov: *Mater. Lett.* **118** (2014) 111–114.
- 68) N.Q. Chinh, T. Csanádi, T. Györi, R.Z. Valiev, B.B. Straumal, M. Kawasaki and T.G. Langdon: *Mater. Sci. Eng. A* **543** (2012) 117–120.
- 69) N.Q. Chinh, T. Csanádi, J. Gubicza and R.Z. Valiev: *MRS Commun.* **9** (2019) 310–314.
- 70) N.Q. Chinh and P. Szommer: *Mater. Sci. Eng. A* **611** (2014) 333–336.
- 71) H. Mehrer (ed.): *Diffusion in Solid Metals and Alloys*, Landolt-Börnstein, Vol. 26, (Springer, Berlin, 1990).
- 72) I. Kaur, W. Gust and L. Kosma: *Handbook of Interphase and Grain Boundary Diffusion*, (Ziegler Press, Stuttgart, 1989).
- 73) M. Kawasaki and T.G. Langdon: *J. Mater. Sci.* **48** (2013) 4730–4741.
- 74) A. Deschamps, M. Niewczas, F. Bley, Y. Brechet, J.D. Embury, L.L. Sinq, F. Livet and J.P. Simon: *Philos. Mag. A* **79** (1999) 2485–2504.
- 75) H. Okuda, M. Tanaka, K. Osamura and Y. Amemiya: *J. Appl. Crystallogr.* **30** (1997) 592–596.
- 76) Y. Komiya, S. Hirisawa and T. Sato: *J. Jpn. Inst. Light Met.* **56** (2006) 662–666.
- 77) T. Sato: *Nanomaterials*, (Elsevier, New York, 2006) pp. 315–346.
- 78) H. Zhao, Y.Q. Chen, B. Gault, S.K. Makineni, D. Ponge and D. Raabe: *Materials* **10** (2020) 100641.
- 79) S.L. Liu, K. Li, J.B. Lu, G. Sha, J.C. Wang, M.J. Yang, G. Ji, M. Song, J. Wang and Y. Du: *J. Alloy. Compd.* **745** (2018) 644–650.
- 80) R.P. Zhang, S.T. Zhao, J. Ding, Y. Chong, T. Jia, C. Ophus, M. Asta, R.O. Ritchie and A.M. Minor: *Nature* **581** (2020) 283–287.
- 81) Z.Z. Song, R.M. Niu, X.Y. Cui, E.V. Bobruk, M. Murashkin, N.A. Enikeev, R.Z. Valiev, S.P. Ringer and X.Z. Liao: *Scr. Mater.* **210** (2022) 114423.
- 82) F.F. Csikor, C. Motz, D. Weygand, M. Zaiser and S. Zapperi: *Science* **318** (2007) 251–254.
- 83) M.D. Uchic, P.A. Shade and D.M. Dimiduk: *Annu. Rev. Mater. Res.* **39** (2009) 361–386.
- 84) P.D. Ispánovity, I. Groma, G. Györgyi, F.F. Csikor and D. Weygand: *Phys. Rev. Lett.* **105** (2010) 085503.
- 85) J.R. Greer and J.T.M. De Hosson: *Prog. Mater. Sci.* **56** (2011) 654–724.
- 86) T.G. Langdon: *Mater. Sci. Eng. A* **174** (1994) 225–230.
- 87) M. Kawasaki and T.G. Langdon: *J. Mater. Sci.* **42** (2007) 1782–1796.
- 88) O.A. Kaibyshev: *Superplasticity of Alloys, Intermetallides and Ceramics*, (Springer-Verlag, Berlin, Heidelberg, 1992).
- 89) O.A. Kaibyshev, R. Safiullin, R. Lutfullin, O. Valiakmetov, R. Galeev and A. Dutta: *Mater. Sci. Technol.* **22** (2006) 343–348.
- 90) S.X. McFadden, R.S. Mishra, R.Z. Valiev, A.P. Zhilyaev and A.K. Mukherjee: *Nature* **398** (1999) 684–686.
- 91) I. Charit and R.S. Mishra: *Acta Mater.* **53** (2005) 4211–4223.
- 92) I.C. Hsiao and J.C. Huang: *Scr. Mater.* **40** (1999) 697–703.
- 93) K.-T. Park, D.-Y. Hwang and D.H. Shin: *Metall. Mater. Trans. A* **33** (2002) 2859–2867.
- 94) T. Luo, D.R. Ni, P. Xue, Y.Z. Li, B.L. Xiao, Z.Y. Ma, M.J. Fu, X.H. Li and Y.S. Zheng: *Mater. Sci. Eng. A* **727** (2018) 177–183.
- 95) Z.Y. Ma and R.S. Mishra: *Scr. Mater.* **53** (2005) 75–80.
- 96) F.C. Liu, Z.Y. Ma and L.Q. Chen: *Scr. Mater.* **60** (2009) 968–971.
- 97) H.-P. Pu and J.C. Huang: *Scr. Metall. Mater.* **28** (1993) 1125–1130.
- 98) S. Lee, K. Watanabe, K. Matsuda and Z. Horita: *Mater. Trans.* **59** (2018) 1341–1347.
- 99) F.C. Liu and Z.Y. Ma: *Scr. Mater.* **58** (2008) 667–670.
- 100) N.Q. Chinh, M.Y. Murashkin, E.V. Bobruk, J.L. Lábár, J. Gubicza, Zs. Kovács, A.Q. Ahmed, V. Maier-Kiener and R.Z. Valiev: *Mater. Res. Lett.* **9** (2021) 475–482.
- 101) J. Gubicza, M. El-Tahawy, J.L. Lábár, E.V. Bobruk, M.Y. Murashkin, R.Z. Valiev and N.Q. Chinh: *J. Mater. Sci.* **55** (2020) 16791–16805.
- 102) A. Juhász, N.Q. Chinh, P. Tasnádi and I. Kovács: *J. Mater. Sci.* **22** (1987) 137–143.
- 103) N.Q. Chinh, J. Illy, A. Juhasz and J. Lendvai: *Phys. Status Solidi A* **149** (1995) 583–599.
- 104) A.D. Kotov, A.V. Mikhaylovskaya and V.K. Portnoy: *Phys. Met. Metallogr.* **115** (2014) 730–735.
- 105) Y.I. Duan, G.F. Xu, X.Y. Peng, Y. Deng, Z. Li and Z.M. Yin: *Mater. Sci. Eng. A* **648** (2015) 80–91.
- 106) K. Higashi, T.G. Nieh, M. Mabuchi and J. Wadsworth: *Scr. Metall. Mater.* **32** (1995) 1079–1084.
- 107) M. Abo-Elkhier and M.S. Soliman: *J. Mater. Eng. Perform.* **15** (2006) 76–80.
- 108) Z. Guan, M. Ren, P. Zhao, P. Ma and Q. Wang: *Mater. Des.* **54** (2014) 906–913.
- 109) X.G. Wang, Q.S. Li, R.R. Wu, X.Y. Zhang and L. Ma: *Adv. Mater. Sci. Eng.* **2018** (2018) 7606140.
- 110) Z. Kovács and N.Q. Chinh: *Scr. Mater.* **188** (2020) 285–289.
- 111) I.J. Polmear: *Light Alloys: Metallurgy of the Light Metals*, 3rd ed., (Arnold, London, 1995).
- 112) A. Azarniya, A.K. Taheri and K.K. Taheri: *J. Alloy. Compd.* **781** (2019) 945–983.
- 113) J. Xu, B. Guo and D. Shan: *Innovative Applications of Ultrafine-Grained Materials, Severe Plastic Deformation Techniques*, ed. by M. Cabibbo, (IntechOpen, London, 2017) Chap. 8, pp. 193–215.